Chronic psychosocial stress compromises the immune response and endochondral ossification during bone fracture healing via β-AR signaling

Melanie Haffner-Luntzer[a,1], Sandra Foertsch[b,1], Verena Fischer[a], Katja Prystaz[a], Miriam Tschaffon[a], Yvonne Mödinger[a], Chelsea S. Bahney[c], Ralph S. Marcucio[c], Theodore Miclau[c], Anita Ignatius[a,1], and Stefan O. Reber[b,1,2]

[a]Institute of Orthopaedic Research and Biomechanics, University Medical Center Ulm, 89081 Ulm, Germany; [b]Laboratory for Molecular Psychosomatics, Department of Psychosomatic Medicine and Psychotherapy, University of Ulm, 89081 Ulm, Germany; and [c]Orthopaedic Trauma Institute, Department of Orthopaedic Surgery, University of California, San Francisco, CA 94110

Edited by Bruce S. McEwen, The Rockefeller University, New York, NY, and approved March 12, 2019 (received for review November 27, 2018)

Chronic psychosocial stress/trauma represents an increasing burden in our modern society and a risk factor for the development of mental disorders, including posttraumatic stress disorder (PTSD). PTSD, in turn, is highly comorbid with a plethora of inflammatory disorders and has been associated with increased bone fracture risk. Since a balanced inflammatory response after fracture is crucial for successful bone healing, we hypothesize that stress/trauma alters the inflammatory response after fracture and, consequently, compromises fracture healing. Here we show, employing the chronic subordinate colony housing (CSC) paradigm as a clinically relevant mouse model for PTSD, that mice subjected to CSC displayed increased numbers of neutrophils in the early fracture hematoma, whereas T lymphocytes and markers for cartilage-to-bone transition and angiogenesis were reduced. At late stages of fracture healing, CSC mice were characterized by decreased bending stiffness and bony bridging of the fracture callus. Strikingly, a single systemic administration of the β-adrenoreceptor (AR) blocker propranolol before femur osteotomy prevented bone marrow mobilization of neutrophils and invasion of neutrophils into the fracture hematoma, both seen in the early phase after fracture, as well as a compromised fracture healing in CSC mice. We conclude that chronic psychosocial stress leads to an imbalanced immune response after fracture via β-AR signaling, accompanied by disturbed fracture healing. These findings offer possibilities for clinical translation in patients suffering from PTSD and fracture.

bone fracture healing | chronic stress | inflammation | adrenoreceptor signaling | trauma

Chronic psychosocial stress represents an increasingly recognized societal burden and a recognized risk factor for the development of numerous mental disorders, including posttraumatic stress disorder (PTSD) (1, 2). This disorder has a high prevalence in western countries, is strongly comorbid with various somatic pathologies (3, 4), and has been associated with bone disorders and increased bone fracture risk in a number of clinical studies (3–7). A clinically relevant mouse model for social stress-associated PTSD is the chronic subordinate colony housing (CSC) paradigm, in which stress is induced in male mice by exposing them to a dominant mouse male aggressor. Nineteen days of CSC exposure induce hyperactivation of the sympathetic nervous system (SNS) and hypoactivation of the hypothalamic–pituitary–adrenal (HPA) axis, in line with what has been shown in patients with PTSD (8). In detail, this is indicated by increased plasma norepinephrine (NE) concentrations, as well as lower basal evening and unaffected basal morning plasma corticosterone (CORT) concentrations following 19 d of CSC exposure (8). Moreover, CSC mice display increased anxiety-related behavior (9) and increased myelopoiesis in the bone marrow (10). Importantly, we further revealed recently that cartilage-to-bone transition during growth plate endochondral ossification is disturbed in CSC versus single-housed control (SHC) mice and that catecholamines released locally in the bone marrow might underlie these negative stress consequences (11). As the process of secondary bone healing after fracture mimics the endochondral ossification process during longitudinal bone growth, we hypothesize that CSC exposure might also compromise bone fracture healing. This hypothesis is further substantiated by our own previous findings demonstrating that CSC exposure promotes systemic immune activation in mice (8), while a balanced inflammatory response after bone fracture is crucial for successful bone healing (12–14). Systemic immune activation, indicated by higher serum levels of proinflammatory cytokines such as interleukin 6 (IL-6) and increased numbers of circulating immune cells (15), has also been shown in individuals suffering from stress-related disorders, including PTSD. β1/β2-adrenoreceptor (AR) signaling promotes both stress-induced emigration of myeloid cells into the circulation, as well as stress-induced activation of myeloid function (16, 17).

Therefore, the aim of the current study was to test the hypothesis that chronic psychosocial stress affects the inflammatory response induced by femur fracture and, consequently, disturbs the bone healing process via β-AR signaling.

Results

CSC Increased Anxiety and Caused Typical Signs of Chronic Psychosocial Stress. Confirming the reliability of our mouse model, the open field/novel object (OF/NO) (*SI Appendix*, Fig. S1) test revealed increased anxiety-related behavior following CSC exposure, which was indicated by a significantly increased time CSC versus SHC

Significance

Our results show that one single systemic administration of the β-adrenoreceptor blocker propranolol prior to femur osteotomy in psychosocially stressed mice prevents stress-induced bone marrow mobilization of neutrophils and their immigration into the early fracture hematoma, as well as the decrease in bending stiffness and bony bridging of the fracture callus, which indicated a compromised fracture healing in stressed mice. These findings offer possibilities for clinical translation in patients suffering from posttraumatic stress disorder and fracture.

Author contributions: M.H.-L., S.F., A.I., and S.O.R. designed research; M.H.-L., S.F., V.F., K.P., M.T., and Y.M. performed research; C.S.B., R.S.M., and T.M. contributed new reagents/analytic tools; M.H.-L., S.F., V.F., K.P., M.T., Y.M., C.S.B., R.S.M., T.M., A.I., and S.O.R. analyzed data; and M.H.-L., S.F., A.I., and S.O.R. wrote the paper.

The authors declare no conflict of interest.

This article is a PNAS Direct Submission.

[1]M.H.-L., S.F., A.I., and S.O.R. contributed equally to this work.

[2]To whom correspondence should be addressed. Email: stefan.reber@uniklinik-ulm.de.

This article contains supporting information online at www.pnas.org/lookup/suppl/doi:10.1073/pnas.1819218116/-/DCSupplemental.

Published online April 4, 2019.

mice spent in one of the four corners of the arena during OF exposure (*SI Appendix*, Fig. S2 *A–C*). Moreover, the time spent in the inner zone of the arena was decreased by trend and distance moved significantly in CSC versus SHC mice during 5 min of NO exploration, while the time spent in one of the four corners of the arena was significantly increased in CSC versus SHC mice (*SI Appendix*, Fig. S2 *D–F*). CSC versus SHC mice in the current study showed a comparable body, significantly increased adrenal and/or decreased thymus weight at 3 h, day 1 (d1) and d3 after surgery (*SI Appendix*, Table S1). Body weight of CSC mice was significantly increased compared with SHC mice at d10 and d21, which is in line with previous studies (9). Thymus weight was increased significantly in CSC versus SHC mice on d10, but was comparable on d1 and d21 after femur osteotomy.

CSC Led to an Imbalanced Inflammatory Response After Fracture. Before fracture, CSC versus SHC mice displayed significantly increased plasma keratinocyte chemoattractant [KC, also known as chemokine (C-X-C motif) ligand 1 (CXCL1)], IL-6, and monocyte chemoattractant protein 1 (MCP-1) levels, whereas all other measured cytokines did not differ (Fig. 1 *A–C*). In the bone marrow, CSC mice displayed significantly increased numbers of $Ly6G^+$ neutrophils, whereas $CD19^+$ B lymphocytes were significantly reduced compared with SHC mice. Numbers of $F4/80^+$ macrophages and T lymphocytes were unaltered (Fig. 1*D*).

Three hours after fracture, CSC mice displayed significantly reduced plasma KC and IL-6 levels compared with SHC mice, whereas all other cytokines did not differ (Fig. 1 *E–G*). Furthermore, IL-6 cytokine concentrations locally in the fracture hematoma were significantly reduced in CSC versus SHC mice, whereas all other cytokines were unaltered (Fig. 1 *H–J*).

Twenty-four hours after fracture, plasma cytokine concentrations were similar between CSC and SHC mice (Fig. 1 *K–M*) and there were no significant differences in $Ly6G^+$ cells in the contralateral bone marrow (Fig. 1*N*, inlay) between CSC and SHC mice. Locally in the fracture hematoma, CSC mice displayed significantly increased numbers of $Ly6G^+$ neutrophils, whereas both $CD8^+$ and $CD4^+$ T lymphocyte numbers were significantly reduced. Numbers of $F4/80^+$ macrophages and $CD19^+$ B lymphocytes did not differ between the groups (Fig. 1*N*), indicating an increased recruitment of $Ly6G^+$ cells from the bone marrow of CSC mice to the fracture hematoma.

On d3 after fracture, the number of $Ly6G^+$ neutrophils remained by trend higher in the callus of CSC versus SHC mice, whereas

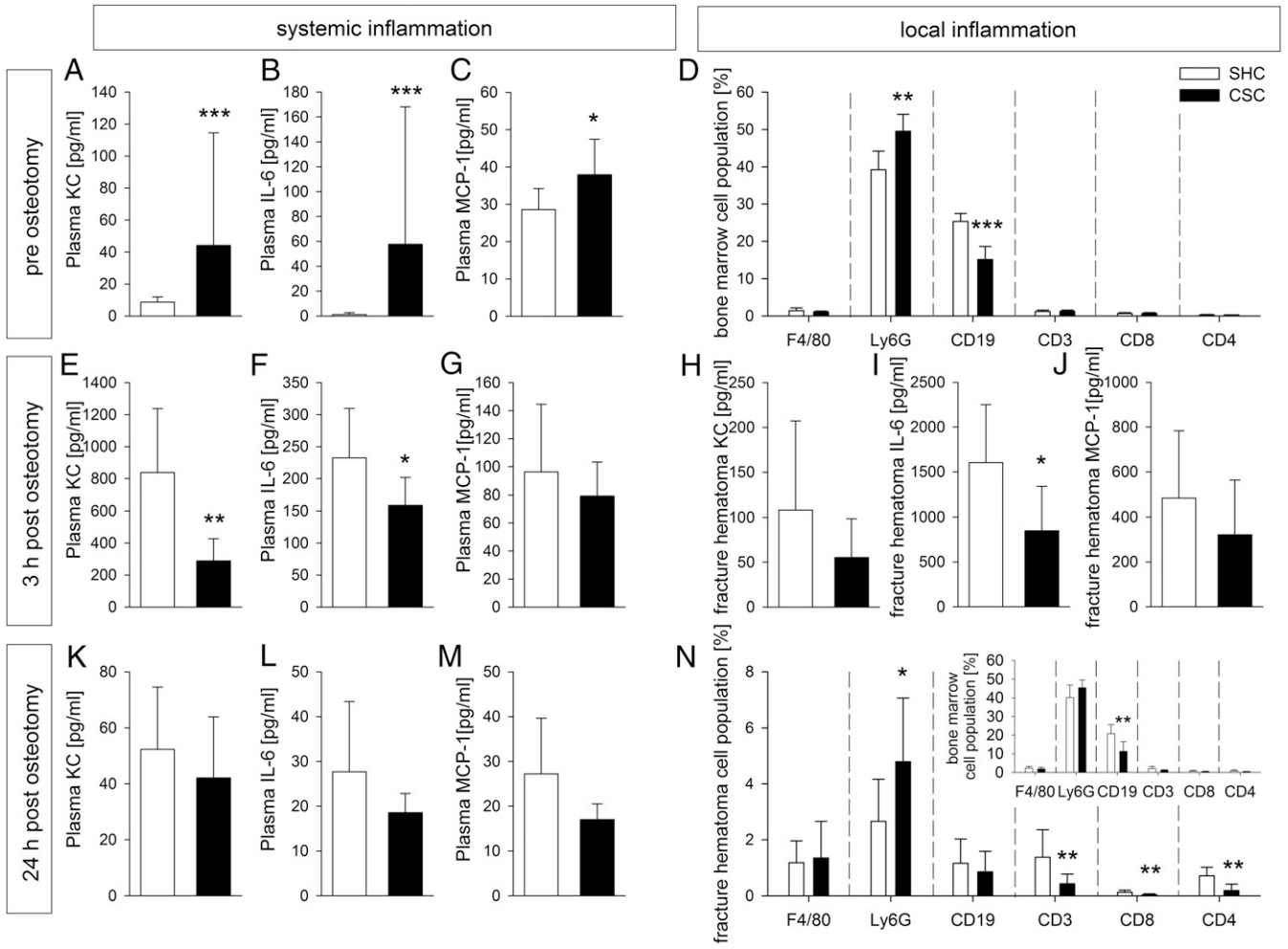

Fig. 1. Inflammatory response toward femur osteotomy following 19 d of CSC housing. (*A*) Plasma KC, (*B*) IL-6, and (*C*) MCP-1 concentrations of SHC and CSC mice after 19 d of stressor exposure. (*D*) Proportion of bone marrow cell populations in SHC and CSC mice on d20 of CSC exposure. (*E*) Plasma KC, (*F*) IL-6, and (*G*) MCP-1 concentrations, as well as (*H*) KC, (*I*) IL-6, and (*J*) MCP-1 concentrations in the fracture hematoma 3 h after femur osteotomy in SHC and CSC mice. (*K*) Plasma KC, (*L*) IL-6, and (*M*) MCP-1 concentrations 24 h after femur osteotomy in SHC and CSC mice. (*N*) Proportion of fracture hematoma and bone marrow (inlay) cell populations in SHC and CSC mice 24 h after femur osteotomy. Data are presented as mean + SD. SHC, $n = 8$; CSC, $n = 8$. *$0.05 > P > 0.01$; **$0.01 > P > 0.001$; ***$P < 0.001$.

numbers of $CD8^+$ T lymphocytes were still significantly lower (Fig. 2 *A*, *B*, *D*, and *E*). Numbers of $F4/80^+$ macrophages did not differ between the groups (Fig. 2 *C* and *F*). No $CD4^+$ T lymphocytes were detectable in the fracture callus at this time point. Furthermore, tyrosine hydroxylase (TH) expression was significantly increased in the granulation tissue surrounding the fracture gap in CSC versus SHC mice both on the gene (Fig. 2*G*) and protein expression levels (Fig. 2*H*), indicating an increased local activation of catecholamine synthesis in CSC mice. Importantly, double staining of TH and Ly6G in the fracture callus (d3 after fracture) revealed 100% colocalization of all TH signals with Ly6G signals (Fig. 2*I*).

CSC Disturbed the Endochondral Ossification Process During Fracture Healing. On d10 after surgery, the relative bone, relative cartilage, relative fibrous tissue, and entire callus areas did not differ between CSC and SHC mice (Fig. 3 *A*–*E*). This indicates that intramembranous ossification taking place at the rims of the fracture callus and chondrocyte proliferation during endochondral ossification occurring in the middle of the fracture callus were not disturbed by prior chronic psychosocial stress. However, immunohistochemical staining for cartilage-to-bone transition and angiogenic markers Sox2, Runx2, and VEGF revealed reduced expression in hypertrophic chondrocytes in the fracture callus (Fig. 3 *G*–*I*). This was confirmed on the gene-expression level (Fig. 3*F*) by laser capture microdissection (LCM) of transition zone tissue (*SI Appendix*, Fig. S3*A*). Furthermore, histological analysis of the cartilage-to-bone transition zone in the fracture callus revealed a reduced vascular area in CSC compared with SHC mice (Fig. 3 *J* and *K*), suggesting reduced neoangiogenesis and disturbed chondrocyte transdifferentiation to osteoblasts in stressed mice. To confirm this hypothesis, we analyzed the fracture callus composition on d21 after surgery. Indeed, μCT analysis revealed reduced bone volume ratios in the fracture callus of CSC versus SHC mice, whereas callus volumes did not differ (Fig. 4 *B*, *C*, and *E*). Furthermore, tissue mineral densities were significantly reduced in CSC compared with SHC mice (Fig. 4*D*). Histomorphometrical analyses revealed reduced relative bone area and increased relative cartilage area in the fracture callus of CSC versus SHC mice, whereas relative fibrous tissue area did not differ significantly (Fig. 4 *F*–*H*). Strikingly, flexural rigidity of fractured femurs was significantly reduced in CSC versus SHC mice (Fig. 4*A*), indicating that disturbed cartilage-to-bone transition results in a poor functional fracture healing outcome. To ensure that the compromised fracture healing in CSC mice was not mediated by differences in general locomotor activity, 24-h home cage activity was assessed directly after surgery as well as in the second and third weeks following fracture. Importantly, no differences between SHC and CSC mice were measured (*SI Appendix*, Fig. S2*G*). Of note, the β2-AR is expressed in the early fracture calli of SHC and CSC mice with femoral osteotomies (*SI Appendix*, Fig. S3*B*), with double stainings on the fracture calli of d10 after surgery revealing, at least to some extent, in both groups colocalization of β2-AR and ectonucleotide pyrophosphate/phosphodiesterase 1 (ENPP1), a marker for chondrocytes in the fracture callus (Fig. 3*L*).

Effects of CSC on the Inflammatory Response After Fracture Are Mediated by β-AR Signaling. Given that β1/β2-AR signaling promotes the stress-induced increase in circulating neutrophils, aggravation of neutrophil invasion into inflamed tissues, and activation of neutrophil function (16, 17), we hypothesized catecholamines via the β1/β2-AR signaling pathway to mediate increased numbers of $Ly6G^+$ neutrophils in the fracture hematoma of CSC versus SHC mice. To test this, we treated a subset of SHC and CSC mice systemically (s.c.) with 10 mg/kg propranolol (18), an unspecific β1/β2-AR blocker, immediately before femur osteotomy, and assessed the immune-cell populations in the fracture hematoma and the bone marrow on d1 after fracture. Consistent with our hypothesis, propranolol treatment abrogated all CSC-induced differences in the immune-cell composition of the fracture callus (Fig. 5*A*). In contrast, $Ly6G^+$ cells were still significantly increased in the contralateral bone marrow of CSC mice injected with propranolol on d1 after fracture, indicating that the increased numbers of $Ly6G^+$ cells in the fracture hematoma of CSC versus SHC mice is indeed mediated by β-AR signaling (Fig. 5*B*).

Interestingly, one single systemic administration of propranolol before femoral osteotomy ameliorated the CSC effects on flexural rigidity, bone volume/total volume (BV/TV), and bone mineral density (BMD) in the fracture callus on d21 following fracture (Fig.

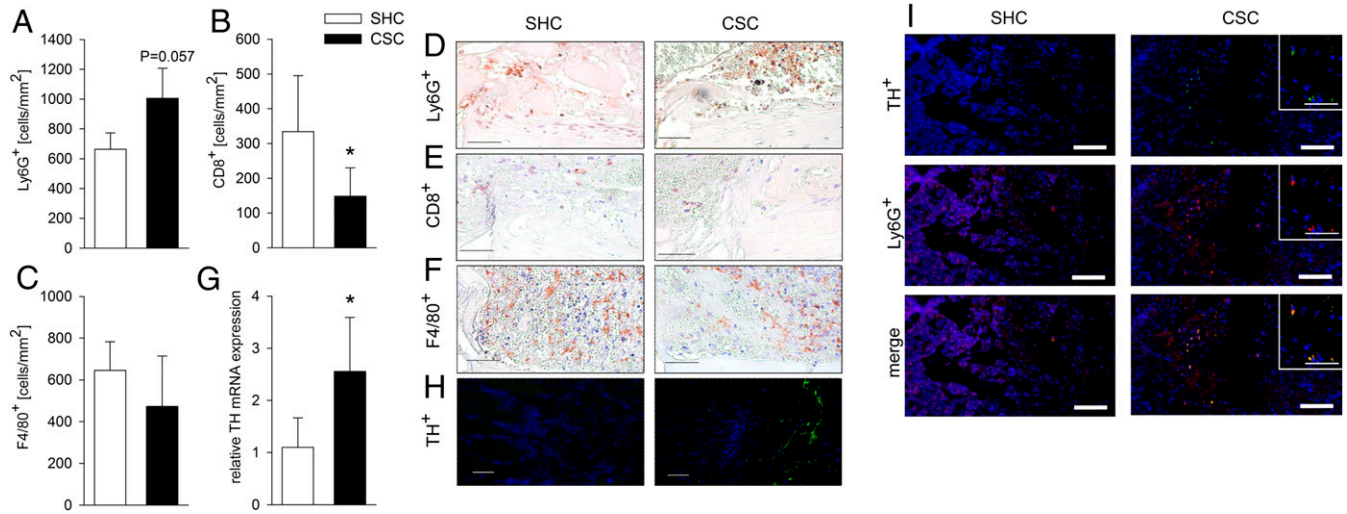

Fig. 2. Immune response in the fracture callus 3 d after femur osteotomy following 19 d of CSC housing. (*A*) Quantification of $Ly6G^+$, (*B*) $CD8^+$, and (*C*) $F4/80^+$ cells in the fracture callus of SHC and CSC mice on d3 after fracture. (*D*) Representative image of fracture callus stained for Ly6G (scale bars: 50 μm), (*E*) CD8 (scale bars: 50 μm), and (*F*) F4/80 (scale bars: 50 μm) of SHC and CSC mice. (*G*) Relative gene expression of TH analyzed by qPCR from fracture hematoma homogenates. Values were normalized to B2M. (*H*) Representative image of fracture callus stained for TH in SHC and CSC mice on d3 after femur osteotomy. (Scale bars: 50 μm.) (*I*) Representative images of fracture calli from SHC (*Left*) and CSC (*Right*) mice on d3 after fracture, double-stained for TH and Ly6G: TH (*Upper*), Ly6G (*Middle*), merge (*Lower*). (Scale bars: 100 μm; inlay: 50 μm.) Data are presented as mean + SD. SHC, $n = 4$–7; CSC, $n = 4$–7. *$0.05 > P > 0.01$.

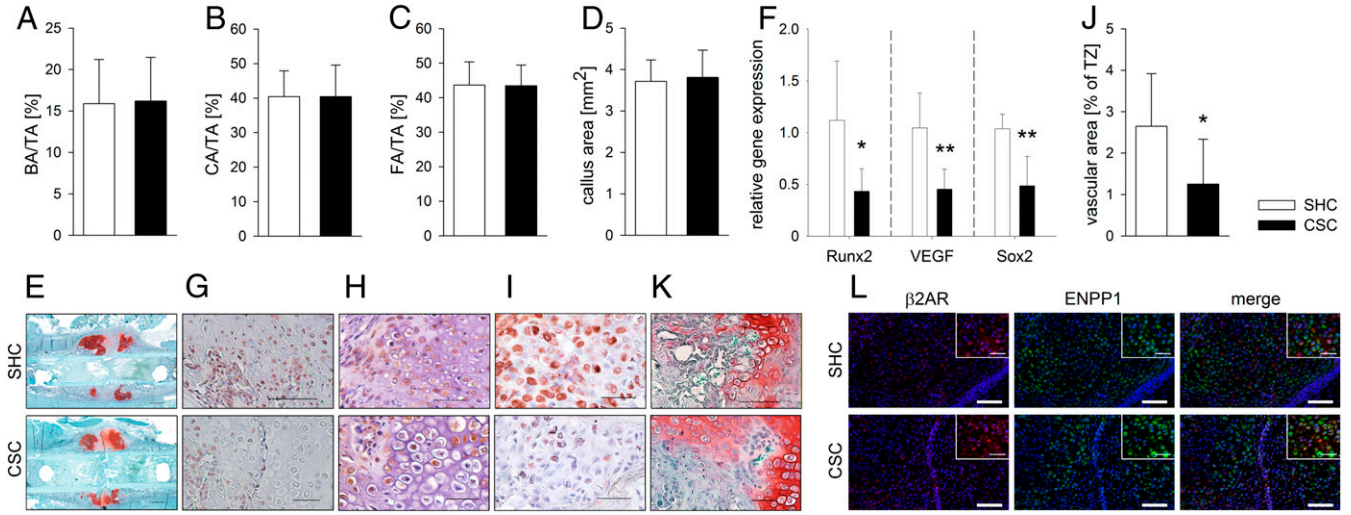

Fig. 3. Callus composition and vascularization on d10 after femur osteotomy following 19 d of CSC housing. (*A*) Bone area/total area (BA/TA) ratio, (*B*) cartilage area/total area (CA/TA) ratio, (*C*) fibrous tissue area/total area (FA/TA) ratio, and (*D*) whole callus area of SHC and CSC mice on d10 after fracture. (*E*) Representative staining of fracture calli stained with Safranin-O. (Scale bars: 500 μm.) (*F*) Relative gene expression of Runx2, VEGF, and Sox2 analyzed by qPCR following LCM of the cartilage-to-bone transition zone of the fracture callus. Values were normalized to B2M. (*G*) Representative image of fracture callus stained for Runx2 (scale bars: 50 μm), (*H*) VEGF (scale bars: 50 μm), and (*I*) Sox2 (scale bars: 100 μm) in SHC and CSC mice on d10 after fracture. (*J*) Relative vascular area of transition zone. (*K*) Representative image of Safranin-O staining of the transition zone in SHC and CSC mice on d10 after fracture. (Scale bars: 50 μm.) (*L*) Representative images of fracture calli from SHC and CSC mice on d10 after fracture, double stained for β2-AR and ENPP1: β2-AR (*Left*), ENPP1 (*Middle*), merge (*Left*). (Scale bars: 100 μm and inlay, 50 μm.) Data are presented as mean + SD. SHC, $n = 5–8$; CSC, $n = 5–8$. *$0.05 > P > 0.01$; **$0.01 > P > 0.001$.

5 *C–G*). This suggests that a β-AR–mediated disturbance of early inflammatory processes during fracture healing is causally involved in the compromised fracture healing seen in CSC mice following chronic psychosocial stress, since the plasma half-life of propranolol is 6 h. Consistently, histomorphometric analysis revealed that a single injection of propranolol before femoral osteotomy also abolished CSC effects on relative bone and cartilage area in the fracture callus on d21 after fracture (Fig. 5 *H–J*). Physiological parameters (*SI Appendix*, Table S1) as well as the 24-h home cage activity (*SI Appendix*, Fig. S2*H*) did not differ between propranolol-treated SHC and CSC mice on d21 after fracture.

Discussion

Psychosocial stress is a well-known risk factor for PTSD and other mental pathologies, which are closely associated with chronic low-grade inflammation and various somatic comorbidities, including disturbed bone homeostasis and increased fracture risk (1–7). In the current study, we used an established animal model for PTSD to show that chronic psychosocial stress compromises both early inflammatory processes as well as endochondral ossification during bone fracture healing in mice and that both processes were mediated by β-AR signaling.

In line with our previous studies (19, 20), mice exposed to the CSC paradigm in the current study developed systemic low-grade inflammation, indicated by increased levels of KC, IL-6, and MCP-1 on d19 of CSC, i.e., 1 d before femur osteotomy. Interestingly, 3 h after fracture CSC mice appeared to be unable to properly respond to the proinflammatory stimulus of the fracture, because cytokine levels rose in SHC but not CSC mice. As a consequence, systemic KC and IL-6 and local IL-6 concentrations were lower in CSC compared with SHC mice 3 h after fracture. KC and IL-6 are important cytokines for recruitment of neutrophils to the site of inflammation (21) and we showed previously that blocking classical IL-6 signaling during the early inflammatory phase of fracture healing led to diminished neutrophil infiltration to the fracture callus, accompanied by disturbed fracture healing (13). Of note, in contrast to single trauma models, blocking of IL-6 transsignaling accelerated fracture healing in a combined trauma model with femur fracture and thorax trauma (22). Surprisingly and in contrast to these previous single trauma studies, CSC mice in the current study displayed increased numbers of $Ly6G^+$ cells in the fracture hematoma, despite systemically and locally reduced IL-6 levels. As outlined in detail in two recent review articles (23, 24), an alternative factor involved the recruitment of stress-mobilized neutrophils

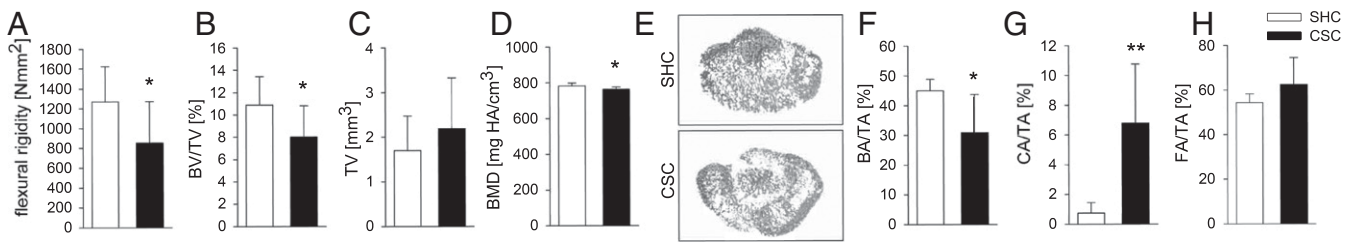

Fig. 4. Fracture callus composition on d21 after femur osteotomy following 19 d of CSC housing. (*A*) Flexural rigidity, (*B*) BV/TV ratio, (*C*) tissue volume, (*D*) BMD, and (*E*) representative μCT 3D reconstructions of the periosteal callus of SHC and CSC mice on d21 after femur osteotomy. (*F*) BA/TA ratio, (*G*) CA/TA ratio, and (*H*) FA/TA ratio. Data are presented as mean + SD. SHC, $n = 8$; CSC, $n = 7–8$. *$0.05 > P > 0.01$; **$0.01 > P > 0.001$.

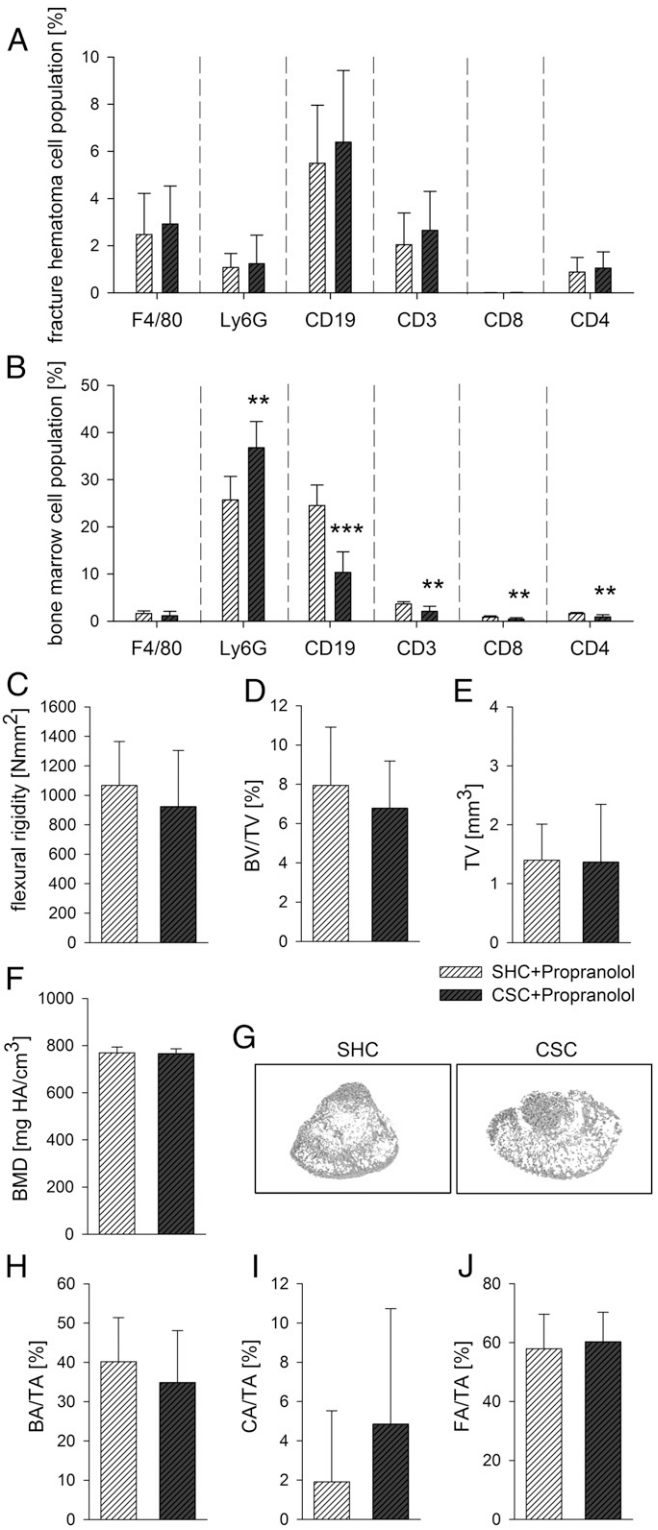

Fig. 5. Influence of propranolol on inflammatory response 24 h and fracture callus composition 21 d after femur osteotomy following 19 d of CSC housing. (*A*) Proportion of fracture hematoma and (*B*) bone marrow cell populations in SHC and CSC mice 24 h after treatment with propranolol directly before femur osteotomy. (*C*) Flexural rigidity, (*D*) BV/TV ratio, (*E*) tissue volume, (*F*) BMD, and (*G*) representative μCT 3D reconstructions of the periosteal callus of SHC and CSC mice on d21 after femur osteotomy treated with propranolol before osteotomy. (*H*) BA/TA ratio, (*I*) CA/TA ratio, and (*J*) FA/TA ratio. Data are presented as mean + SD. SHC, n = 7–8; CSC, n = 6–8. $^{**}0.01 > P > 0.001$; $^{***}P < 0.001$.

to the fracture hematoma might be the CC-chemokine ligand 2 (CCL2; also known as MCP-1). CCL2 has been shown to mediate recruitment of activated myeloid cells to the brain under conditions of stress and peripheral inflammation (25, 26), and, in line with our own previous studies (27), was systemically increased in mice exposed to 19 d of CSC. Furthermore, CCL2 regulates the infiltration of inflammatory cells to the fracture callus (28). Of note in this context, NE release by sympathetic nerve fibers during chronic variable stress signals bone marrow niche cells to decrease CXCL12 levels through the β3-adrenoreceptor, resulting in increased hematopoietic stem cell proliferation and release of neutrophils and inflammatory monocytes (29). In addition, also β1/β2-AR signaling has been proposed to mediate the stress-induced increase in circulating neutrophils, aggravation of neutrophil invasion into inflamed tissues, and activation of neutrophil function (16, 17). In line with the latter, β1/β2-AR blockade immediately before femur osteotomy prevented mobilization of $Ly6G^+$ cells from the bone marrow and, consequently, their migration into the fracture hematoma. This was indicated by increased $Ly6G^+$ cell numbers in the bone marrow of the intact femur of propranolol-treated CSC mice on d1 after fracture and normal levels of $Ly6G^+$ cells in the fracture hematoma. Interestingly, propranolol treatment also abolished the reduced numbers of T lymphocytes in the fracture hematoma of CSC mice. Since it was shown previously that chronic psychosocial stress can induce $CD11b^+/Ly6G^+/Ly6C^+$ myeloid derived suppressor cells (MDSCs) in the bone marrow, which are known to suppress T cell proliferation (10, 30), we hypothesize that besides neutrophils, a proportion of the $Ly6G^+$ cells found in the fracture hematoma of CSC mice represent MDSCs. By blocking β-AR signaling, the exaggerated mobilization and, consequently, migration of MDSCs to the fracture hematoma in CSC mice might be normalized, thereby explaining the lack of an effect on T cell proliferation and normal numbers of T lymphocytes in the fracture callus of CSC mice injected with propranolol. However, it is also known that IL-6 classic signaling is important for recruitment of T cells to the fracture hematoma (13), therefore the reduced levels of IL-6 present in the fracture hematoma of CSC mice might also account for the reduced numbers of T lymphocytes. In conclusion, chronic psychosocial stress seems to shift the immune response after fracture toward the innate arm of immunity, thereby suppressing its adaptive response, both mediated by β1/β2-AR signaling. A balanced presence and activation of neutrophils was shown to be crucial for proper fracture healing (12, 14, 31). Neutrophils can act in both a proregenerative manner by providing a fibronectin-rich matrix for proper callus development (32) or can provoke negative effects by secreting reactive oxygen species and other cytotoxic compounds, including hypochloride. Therefore, increased numbers of neutrophils or overactivation of these cells can cause tissue damage and delay tissue regeneration (33, 34). Alternatively, as TH^+ cells found exclusively in the fracture callus of CSC but not SHC mice were all expressing Ly6G, the stress-induced and β1/β2-AR–mediated increase in neutrophils in the fracture callus of CSC mice might result in elevated local catecholamine levels, known to have profound effects on neuronal control of bone formation (35). T cells also play an important role during fracture healing. It was, for instance, shown previously that terminally differentiated $CD8^+$ T lymphocytes negatively affect fracture healing (36). However, because we found disrupted fracture healing in CSC mice, we believe that the negative effects of enhanced neutrophil recruitment to the site of injury exceeded the possible positive effects of reduced $CD8^+$ T cells. Of note, as human neutrophils show sex-specific differences in β2-AR binding and β2-AR–induced nondirected locomotion (37), it might be of interest to also extend the present findings to female mice using chronic psychosocial stress models that are not based on territorial aggression and hierarchy establishment.

CSC mice displayed reduced expression of the angiogenic and cartilage-to-bone transition markers, in the fracture callus on d10 after femur osteotomy. Furthermore, vascularization was reduced in the transition zone from cartilage to bone in the callus. In line with these findings, which suggest an overall compromised fracture healing in CSC mice, bony bridging, mineralization, and flexural rigidity of the fracture callus were lower in CSC compared with SHC mice on d21 after surgery. In addition, persistent cartilage was present in the fracture callus of CSC but not SHC mice, clearly indicating disturbed endochondral ossification during fracture healing in stressed mice. Noteworthy in this context, it was shown that angiogenic factors such as VEGF and chondrocyte dedifferentiation transcription factors like Sox2 are critical for chondrocyte transdifferentiation to osteoblasts (38), which is crucial for endochondral fracture healing (39). Conditional deletion of Sox2 during fracture healing led to persistent cartilage in the fracture callus and decreased bone formation (38). As one single dose of propranolol injected before femoral osteotomy not only abrogated early CSC effects on inflammatory processes, but also improved compromised late fracture healing, and as the β2-AR on chondrocytes is discussed as the major receptor involved in neuronal control of bone formation (35), it is likely that locally secreted catecholamines from stress-induced and β1/β2-adrenoreceptor signaling-mediated TH^+/$Ly6G^+$ neutrophils disturbed proper endochondral ossification via the β2-AR on chondrocytes. Support for this hypothesis is provided by double stainings on d10-fracture calli of SHC and CSC mice, illustrating colocalization of the β2-AR and ENPP1 in both groups.

Of note, propranolol treatment might also have systemic effects, which could possibly influence fracture healing. It was shown that propranolol influences heart rate, blood pressure, activity, tissue perfusion, and tissue oxygen consumption (40). However, since we injected propranolol only once immediately prior to fracture and as we did not detect differences in general locomotion on d0/1, d7/8, and d14/15 after fracture, these effects might be of minor importance in our study. Furthermore, it was shown previously that catecholamine signaling and signaling of other neurotransmitters does not only influence immune cells but also bone cells. Injections with propranolol showed antiosteoporotic effects in rodents (41) and reduced fracture risk in humans (42–44), although callus development during fracture healing was not influenced (18). Absence of the neurotransmitter substance P reduced mineralization during late osteoblast differentiation (45) and delayed fracture healing (46).

Importantly, chronic psychosocial stress also impairs other regenerative processes. For example, examination and caregiving stress in humans as well as social isolation stress in mice have been linked to compromised mucosal (47, 48) and/or cutaneous wound healing (49). Of note in the context of the current study, propranolol administration and, thus, blockade of β-AR signaling, before wound healing ameliorated detrimental effects of chronic stress on cutaneous wound healing in mice (50).

In conclusion, our results show that one single systemic administration of the β1/β2-AR blocker propranolol immediately before femur osteotomy in psychosocially stressed mice prevents stress-induced bone marrow mobilization of neutrophils and, consequently, their immigration into the early fracture hematoma, as well as the decrease in bending stiffness and bony bridging of the fracture callus, indicating a compromised fracture healing. Thus, our results might have significant clinical relevance in terms of future treatment strategies to improve fracture healing in patients with PTSD. This is of particular interest, given that PTSD and fractures are strongly comorbid in soldiers (51), people living in war zones (52), and children subjected to physical abuse (53), among others, and there is clinical evidence that fracture healing is delayed in patients with PTSD after forearm fracture (54). This represents a potential area for further basic and clinical research work. Furthermore, it might be of importance to investigate the effects of chronic psychosocial stress on fracture healing in severely injured trauma individuals. As injury severity influences inflammation and fracture healing outcome (13, 22), it might be possible that the negative impact of chronic stress on fracture healing are even more potent in subjects with higher physical trauma load.

Methods

Animals. Male C57BL/6N mice (experimental mice, 19–22 g) and male CD-1 (dominant resident mice, 30–35 g) mice were obtained from Charles River Laboratories. All mice were kept under standard laboratory conditions (12-h light/12-h dark cycle, lights on at 6:00 AM, 22 °C, 60% humidity) and had free access to tap water and standard mouse diet.

Study Approval. All animal experiments were in compliance with international regulations for the care and use of laboratory animals [ARRIVE guidelines and European Union (EU) Directive 2010/63/EU for animal experiments] with the approval of the local ethical committee (No. 1219, Regierungspräsidium Tübingen, Germany).

Experimental Design. Different sets of 7-wk-old mice ($n = 8$ per group and time point) were either chronically stressed by a 19-d exposure to the CSC paradigm or SHC. On d20, a standardized femur osteotomy of the right femur was performed according to an establish protocol (55) and afterward all mice were kept individually for the different healing phases. For further details see *SI Appendix*, Fig. S1.

CSC Paradigm. The CSC paradigm was performed as described previously (19, 20, 56). Briefly, after being single-housed for 1 wk after arrival, experimental CSC mice were housed together with a dominant male CD-1 mouse for 19 consecutive days to induce chronic psychosocial stress. To avoid habituation, CSC mice were introduced into the home cage of a novel dominant male mouse on d8 and d15 of the CSC procedure. Except for a weekly change of bedding, the respective SHC mice remained undisturbed in their home cages for 19 consecutive days. Single housing was demonstrated to be the adequate control group for the CSC paradigm, because group housing itself is able to promote typical CSC-induced physiological changes (57). The OF/NO test was performed on d19 of the CSC paradigm in all sets of SHC and CSC mice as previously described (58) with minor modifications. The 24-h home cage locomotion was assessed on d1 after femur osteotomy as well as in the second and third week after fracture.

Propranolol Administration. After successful initiation of anesthesia on d20, mice received a single administration (s.c.) of propranolol (10 mg/kg body weight, dissolved in 0.9% saline) directly before the osteotomy surgery.

OF/NO Test. The OF/NO test was performed on d19 of the CSC paradigm in all sets of SHC and CSC mice as previously described (58) with minor modifications. Briefly, the arena (45 cm height × 27 cm length × 27 cm width) was subdivided into an inner and an outer zone, and the four corners. At the start of the first trial, the experimental mouse was placed into the inner zone of the arena and allowed to explore the arena for 5 min. Immediately after this OF exploration, a plastic round object (diameter, 3.5 cm; height, 1.5 cm) was placed into the center of the inner zone and the mouse explored the arena containing the unfamiliar object for another 5 min. During both trials, the distance moved as well as the time the experimental mouse spent in the four corners were assessed. Furthermore, in the OF test, the time the animals spent in the inner zone of the arena and in the NO test, the time spent at the NO, were investigated. All parameters were analyzed using EthoVision XT (version 9, Noldus Information Technology). The test was performed between 8:00 AM and 12:00 AM under white light conditions (300 lx).

Twenty-Four Hour Home Cage Locomotion. The 24-h home cage locomotion was assessed on d1 after femur osteotomy as well as in the second and third week after fracture. All mice were videotaped between 6:00 PM and 6:00 PM of the following day in their home cage from above and the distance moved was analyzed using EthoVision XT (version 9).

Determination of Body, Adrenal, and Thymus Weights. After decapitation under CO_2 anesthesia in the morning (between 6:00 AM and 10:00 AM) of the respective experiment, the adrenal glands as well as the thymus were removed, pruned of fat, and weighed.

Trunk Blood Sampling. Within 3 min after removing the cage from the animal room, mice were decapitated following brief CO_2 anesthesia. Trunk blood was collected in ethylendiaminetetraacetic acid (EDTA)-coated tubes (Sarstedt) and stored on ice until centrifugation. Tubes were centrifuged at 4 °C (5,000 × *g*, 10 min). Plasma samples were stored at −20 °C until further analysis.

Multiplex Cytokine ELISA. To investigate the effects of CSC on the systemic and local early immune response after fracture (3 h, d1), we assessed cytokine and chemokine concentrations in blood plasma and the fracture hematoma by multiplex immunoassay. The harvested fracture hematoma was lysed in lysis buffer containing protease inhibitors [10 mM Tris, pH 7.5, 10 mM NaCl, 0.1 mM EDTA, 0.5% Triton-X 100, 0.02% NaN3, 0.2 mM phenylmethylsulfonyl fluoride, and Halt Protease and Phosphate Inhibitor Single-Use Mixture (Thermo Fisher Scientific)]. Total fracture hematoma protein concentration was determined by Pierce BCA Protein Assay Kit (Thermo Fisher Scientific). Using a customized mouse Multiplex Cytokine Kit (ProcartaPlex, eBioscience) plasma and fracture hematoma concentrations of IL-6, IL-1β, IL-13, IL-4, CXCL1, MCP-1, and macrophage inflammatory protein 1α (MIP-1α) were determined.

Fluorescence-Activated Cell Sorting. Inflammatory cells in the fracture hematoma on d1 after fracture were analyzed by fluorescence-activated cell sorting (FACS). The fractured femurs and contralateral bone marrow were harvested. The fracture hematoma was passed through a 70-μm cell strainer (Corning, Inc.) to obtain a single-cell suspension and all cells were subjected to erythrolysis. For the identification of macrophages ($F4/80^+$), neutrophils ($Ly\text{-}6G^+$), B lymphocytes ($CD19^+$), T lymphocytes ($CD3^+$), cytotoxic T lymphocytes ($CD3^+$ and $CD8^+$), and T helper lymphocytes ($CD3^+$ and $CD4^+$) the antibodies listed in *SI Appendix*, Table S2 were used. Specific isotype-matched Ig antibodies (*SI Appendix*, Table S2) were used as negative controls. Cells were incubated with the antibodies for 30 min on ice. The 7-aminoactinomycin (7-AAD) (Sigma) was used for dead-cell discrimination. Cells were analyzed using a BD FACSCalibur flow cytometer (BD Bioscience) and FlowJo software v10.

Biomechanical Testing, μCT Analysis, and Histomorphometry. Biomechanical testing of the intact and fractured femurs of mice killed on d21 after fracture was performed using a nondestructive three-point bending test as described previously (55). Afterward, fractured femurs were fixed in 4% paraformaldehyde for 48 h. μCT scanning was performed using the Skyscan 1172, operating at 50 kV and 200 mA. Voxel resolution was set at 8 μm. Three-dimensional analysis was conducted using CTAn and CTVol software according to the American Society for Bone and Mineral Research guidelines (59). The volume of interest was defined as the entire periosteal callus between the two inner pinholes. Tissue mineral density was assessed using two phantoms with defined hydroxyapatite (HA) contents (250 and 750 mg/cm^3). The threshold for mineralized tissue was set at 642 mg HA/cm^3. After μCT scans, right femurs were subjected to decalcified histology as described previously (60). Sections of 7 μm were stained with Safranin O. The amounts of bone, cartilage, and fibrous tissue at d10 and d21 after fracture were determined using image-analysis software (Leica MMAF 1.4.0 Imaging System). Region of interest was the whole fracture callus between the cortices. Vascularization was assessed in the transition zone from cartilage to bone using the Osteomeasure System in Safranin O-stained sections.

Immunohistochemistry and Immunofluorescence Staining. Longitudinal sections of 7 μm were prepared for immunohistochemical and immunofluoresence staining. Staining for Runx2, VEGF, Sox2, Ly6G, F4/80, and CD8, as well as double stainings for TH and Ly6G as well as β2-AR and ENPP1 were performed using the following antibodies: rabbit anti-mouse Runx2 (8486, Cell Signaling), rabbit anti-mouse VEGF (ab46154, Abcam), rat anti-mouse Ly6G (127603, BioLegend), rat anti-mouse F4/80 (ab6640, Abcam), rabbit anti-mouse CD8 (bs-0648R, Bioss), rabbit anti-mouse Sox2 (ab97959, Abcam), goat anti-rabbit IgG-biotin (sc-3840, Santa Cruz), goat anti-rat IgG-biotin (31830, Invitrogen), and horseradish peroxidase-conjugated streptavidin (Zytomed Systems). 3-Amino-9-ethylcarbazol (Zytomed Systems) was used as the chromogen and the sections were counterstained using hematoxylin (Waldeck). Immunofluorescence staining for TH and β2-AR, as well as double stainings for TH and Ly6G and β2-AR and ENPP1 was performed using the following antibodies: rabbit anti-mouse β2-AR antibody (sc-569, Santa Cruz), rabbit anti-mouse TH antibody (AB152, Millipore), rat anti-mouse Ly6G (127632, BioLegend), goat anti-mouse ENPP1/PC1 (SAB 2500355, Sigma), goat-anti rabbit IgG-biotin (sc-3840, Santa Cruz), donkey anti-rabbit IgG AF594 (A21207, Invitrogen), goat anti-rat IgG-biotin (A10517, Life Technologies), donkey anti-goat IgG-biotin (A10518, Life Technologies), and FITC-streptavidin (40201, BioLegend). Species-specific nontargeting immunoglobulins were used as isotype controls.

LCM of Fracture Callus Tissue and RNA Isolation. RNase-free longitudinal paraffin fracture callus sections of 8 μm were prepared for LCM and mounted on 0.05% poly-L-lysine–coated 1.0 PEN membrane slides (Zeiss). Directly after mounting, sections were deparaffinized, rehydrated, and stained with hematoxylin in an RNase-free staining procedure. After dehydrating, sections were air dried for 15 min and directly processed for LCM. LCM was performed with a PALM MicroBeam LCM System (Zeiss) according to the manufacturer's instructions. Speed of laser was set to 59%, energy of laser for cutting was set to 63%, energy of laser for catapulting was set to delta 30, and focus of laser was set to 86%. Transition zone tissue from the cartilaginous to the bony region of the fracture callus (*SI Appendix*, Fig. S3) was cut and collected in adhesive cap tubes (Zeiss). RNA was isolated using the RNEasy FFPE Kit (Qiagen) according to the manufacturer's instructions. Amount and purity of RNA was measured photometrically with a Tecan NanoPlate. Integrity of RNA was determined with 3′/5′ primer PCR assay (61) for β2 microglobulin (B2M) (3′ end primer F: 5′-CTC GGT GAC CCT GGT CTT TC-3′ and R: 5′-TTG AGG GGT TTT CTG GAT AGC A-3′; 5′ end primer F: 5′-TGT CAC TGT GCC CAA TGC TTA-3′ and R: 5′-GAA GTA GCC ACA GGG TTG GG-3′). Integrity was >70% for all samples.

qPCR. Isolated RNA was transcribed into cDNA using the Omniscript Reverse Transcriptase Kit (Qiagen). Quantitative PCR was performed using the Brilliant Sybr Green QPCR Master Mix Kit (Stratagene) according to the manufacturer's protocol in a total volume of 25 μL using the following cycling conditions: 50 °C for 2 min, 95 °C for 2 min, and 50 cycles each consisting of 95 °C for 15 s and 60 °C for 1 min. Then melting curve acquisition was performed (95 °C for 15 s, 60 °C for 1 min, 95 °C for 15 s). *B2M* was used as the housekeeping gene (F: 5′-CCC GCC TCA CAT TGA AAT CC-3′ and R: 5′-TGC TTA ACT CTG CAG GCG TAT-3′). The primers for *VEGF* were 5′-AAA AAC GAA AGC GCA AGA AA-3′ and 5′-AAT GCT TTC TCC GCT CTG AA-3′, for *Runx2* 5′-CCA CCA CTC ACT ACC ACA CG-3′ and 5′-CAC TCT GGC TTT GGG AAG AG-3′, for *Sox2* 5′-CAA AAA CCG TGA TGC CGA CT-3′ and 5′-CGC CCT CAG GTT TTC TCT GT-3′, and for *TH* 5′-AACCCTCCTCACTGTCTCGGGC-3′ and 5′-TCAGACACCCGACGCACAGAACT-3′. Relative gene expression was calculated using the delta–delta CT method with PCR-efficiency correction using LinRegPCR software as described previously (62).

Statistics and Data Availability. All acquired datasets of the present study were tested for normal distribution using the Kolmogorov–Smirnov test using the Lilliefors correction. Outliers in normally distributed datasets were identified using the Grubbs' test and excluded from further analysis. For normally distributed datasets, significance was analyzed using the Student's *t* test for single comparison. Nonnormally distributed datasets were analyzed using the nonparametric Mann–Whitney's *U* test. All results are presented as the mean value and SD. Values of $P \leq 0.05$ were considered to be statistically significant. Results marked with * are $0.05 \geq P \geq 0.01$, ** are $0.01 > P > 0.001$, and *** are $P < 0.001$. Statistical analysis was performed using the software package IBM SPSS statistics (version 25.0).

ACKNOWLEDGMENTS. We thank Marion Tomo, Sevil Essig, Uschi Maile, Iris Baum, and Chérise Grieser (Institute of Orthopedic Research and Biomechanics); Petra Hornischer and Ulrike Binder (Laboratory for Molecular Psychosomatics) for excellent technical support; and Dr. Sybille Ott, Susanna Brämisch, and Ekaterina Merkel from the local animal caretaking facility (Tierforschungszentrum, University Ulm) for their excellent support. This work was supported by the Collaborative Research Centre Grant CRC1149 (funded by the Deutsche Forschungsgemeinschaft, German Research Foundation, Project 251293561).

1. Yehuda R, Seckl J (2011) Minireview: Stress-related psychiatric disorders with low cortisol levels: A metabolic hypothesis. *Endocrinology* 152:4496–4503.
2. Gold PW, Goodwin FK, Chrousos GP (1988) Clinical and biochemical manifestations of depression. Relation to the neurobiology of stress (1). *N Engl J Med* 319:348–353.
3. Gebara MA, et al. (2014) Depression, antidepressants, and bone health in older adults: A systematic review. *J Am Geriatr Soc* 62:1434–1441.
4. Glaesmer H, Kaiser M, Bräehler E, Freyberger HJ, Kuwert P (2012) Posttraumatic stress disorder and its comorbidity with depression and somatisation in the elderly–A German community-based study. *Aging Ment Health* 16:403–412.
5. Calarge CA, et al. (2014) Major depressive disorder and bone mass in adolescents and young adults. *J Bone Miner Res* 29:2230–2237.
6. Zong Y, et al. (2016) Depression is associated with increased incidence of osteoporotic thoracolumbar fracture in postmenopausal women: A prospective study. *Eur Spine J* 25:3418–3423.
7. Glaesmer H, Brähler E, Gündel H, Riedel-Heller SG (2011) The association of traumatic experiences and posttraumatic stress disorder with physical morbidity in old age: A German population-based study. *Psychosom Med* 73:401–406.
8. Reber SO, et al. (2016) Chronic subordinate colony housing paradigm: A mouse model for mechanisms of PTSD vulnerability, targeted prevention, and treatment-2016 Curt Richter award paper. *Psychoneuroendocrinology* 74:221–230.
9. Slattery DA, et al. (2012) Behavioural consequences of two chronic psychosocial stress paradigms: Anxiety without depression. *Psychoneuroendocrinology* 37:702–714.
10. Schmidt D, Peterlik D, Reber SO, Lechner A, Männel DN (2016) Induction of suppressor cells and increased tumor growth following chronic psychosocial stress in male mice. *PLoS One* 11:e0159059.
11. Foertsch S, et al. (2017) Chronic psychosocial stress disturbs long-bone growth in adolescent mice. *Dis Model Mech* 10:1399–1409.
12. Haffner-Luntzer M, Fischer V, Prystaz K, Liedert A, Ignatius A (2017) The inflammatory phase of fracture healing is influenced by oestrogen status in mice. *Eur J Med Res* 22:23.
13. Prystaz K, et al. (2018) Distinct effects of IL-6 classic and trans-signaling in bone fracture healing. *Am J Pathol* 188:474–490.
14. Kovtun A, et al. (2016) The crucial role of neutrophil granulocytes in bone fracture healing. *Eur Cell Mater* 32:152–162.
15. Miller AH, Maletic V, Raison CL (2009) Inflammation and its discontents: The role of cytokines in the pathophysiology of major depression. *Biol Psychiatry* 65:732–741.
16. Hanke ML, Powell ND, Stiner LM, Bailey MT, Sheridan JF (2012) Beta adrenergic blockade decreases the immunomodulatory effects of social disruption stress. *Brain Behav Immun* 26:1150–1159.
17. Deng Q, et al. (2016) Psychological stress promotes neutrophil infiltration in colon tissue through adrenergic signaling in DSS-induced colitis model. *Brain Behav Immun* 57:243–254.
18. Smitham P, et al. (2014) Low dose of propranolol does not affect rat osteotomy healing and callus strength. *J Orthop Res* 32:887–893.
19. Reber SO, et al. (2007) Adrenal insufficiency and colonic inflammation after a novel chronic psycho-social stress paradigm in mice: Implications and mechanisms. *Endocrinology* 148:670–682.
20. Reber SO, Obermeier F, Straub RH, Veenema AH, Neumann ID (2008) Aggravation of DSS-induced colitis after chronic subordinate colony (CSC) housing is partially mediated by adrenal mechanisms. *Stress* 11:225–234.
21. Fielding CA, et al. (2008) IL-6 regulates neutrophil trafficking during acute inflammation via STAT3. *J Immunol* 181:2189–2195.
22. Kaiser K, et al. (2018) Pharmacological inhibition of IL-6 trans-signaling improves compromised fracture healing after severe trauma. *Naunyn Schmiedebergs Arch Pharmacol* 391:523–536.
23. Wohleb ES, McKim DB, Sheridan JF, Godbout JP (2015) Monocyte trafficking to the brain with stress and inflammation: A novel axis of immune-to-brain communication that influences mood and behavior. *Front Neurosci* 8:447.
24. Miller AH, Raison CL (2016) The role of inflammation in depression: From evolutionary imperative to modern treatment target. *Nat Rev Immunol* 16:22–34.
25. Wohleb ES, et al. (2011) β-Adrenergic receptor antagonism prevents anxiety-like behavior and microglial reactivity induced by repeated social defeat. *J Neurosci* 31:6277–6288.
26. Wohleb ES, Powell ND, Godbout JP, Sheridan JF (2013) Stress-induced recruitment of bone marrow-derived monocytes to the brain promotes anxiety-like behavior. *J Neurosci* 33:13820–13833.
27. Langgartner D, Palmer A, Rittlinger A, Reber SO, Huber-Lang M (2018) Effects of prior psychosocial trauma on subsequent immune response after experimental thorax trauma. *Shock* 49:690–697.
28. Xing Z, et al. (2010) Multiple roles for CCR2 during fracture healing. *Dis Model Mech* 3:451–458.
29. Heidt T, et al. (2014) Chronic variable stress activates hematopoietic stem cells. *Nat Med* 20:754–758.
30. Hüsecken Y, et al. (2017) MDSCs are induced after experimental blunt chest trauma and subsequently alter antigen-specific T cell responses. *Sci Rep* 7:12808.
31. Recknagel S, et al. (2013) Systemic inflammation induced by a thoracic trauma alters the cellular composition of the early fracture callus. *J Trauma Acute Care Surg* 74:531–537.
32. Bastian OW, Koenderman L, Alblas J, Leenen LP, Blokhuis TJ (2016) Neutrophils contribute to fracture healing by synthesizing fibronectin+ extracellular matrix rapidly after injury. *Clin Immunol* 164:78–84.
33. Butterfield TA, Best TM, Merrick MA (2006) The dual roles of neutrophils and macrophages in inflammation: A critical balance between tissue damage and repair. *J Athl Train* 41:457–465.
34. Kemmler J, et al. (2015) Exposure to 100% oxygen abolishes the impairment of fracture healing after thoracic trauma. *PLoS One* 10:e0131194.
35. Takeda S, et al. (2002) Leptin regulates bone formation via the sympathetic nervous system. *Cell* 111:305–317.
36. Reinke S, et al. (2013) Terminally differentiated $CD8^+$ T cells negatively affect bone regeneration in humans. *Sci Transl Med* 5:177ra36.
37. de Coupade C, et al. (2004) Beta 2-adrenergic receptor regulation of human neutrophil function is sexually dimorphic. *Br J Pharmacol* 143:1033–1041.
38. Hu DP, et al. (2017) Cartilage to bone transformation during fracture healing is coordinated by the invading vasculature and induction of the core pluripotency genes. *Development* 144:221–234.
39. Zhou X, et al. (2014) Chondrocytes transdifferentiate into osteoblasts in endochondral bone during development, postnatal growth and fracture healing in mice. *PLoS Genet* 10:e1004820.
40. Aguilar-Olivos N, et al. (2014) Hemodynamic effect of carvedilol vs. propranolol in cirrhotic patients: Systematic review and meta-analysis. *Ann Hepatol* 13:420–428.
41. Sato T, Arai M, Goto S, Togari A (2010) Effects of propranolol on bone metabolism in spontaneously hypertensive rats. *J Pharmacol Exp Ther* 334:99–105.
42. Schlienger RG, Kraenzlin ME, Jick SS, Meier CR (2004) Use of beta-blockers and risk of fractures. *JAMA* 292:1326–1332.
43. Bonnet N, Pierroz DD, Ferrari SL (2008) Adrenergic control of bone remodeling and its implications for the treatment of osteoporosis. *J Musculoskelet Neuronal Interact* 8:94–104.
44. Graham S, et al. (2008) The effect of beta-blockers on bone metabolism as potential drugs under investigation for osteoporosis and fracture healing. *Expert Opin Investig Drugs* 17:1281–1299.
45. Niedermair T, Schirner S, Seebröker R, Straub RH, Grässel S (2018) Substance P modulates bone remodeling properties of murine osteoblasts and osteoclasts. *Sci Rep* 8:9199.
46. Niedermair T, et al. (2014) Absence of substance P and the sympathetic nervous system impact on bone structure and chondrocyte differentiation in an adult model of endochondral ossification. *Matrix Biol* 38:22–35.
47. Marucha PT, Kiecolt-Glaser JK, Favagehi M (1998) Mucosal wound healing is impaired by examination stress. *Psychosom Med* 60:362–365.
48. Godbout JP, Glaser R (2006) Stress-induced immune dysregulation: Implications for wound healing, infectious disease and cancer. *J Neuroimmune Pharmacol* 1:421–427.
49. Kiecolt-Glaser JK, Marucha PT, Malarkey WB, Mercado AM, Glaser R (1995) Slowing of wound healing by psychological stress. *Lancet* 346:1194–1196.
50. Romana-Souza B, Porto LC, Monte-Alto-Costa A (2010) Cutaneous wound healing of chronically stressed mice is improved through catecholamines blockade. *Exp Dermatol* 19:821–829.
51. Lee CH, Choi CH, Yoon SY, Lee JK (2015) Posttraumatic stress disorder associated with orthopaedic trauma: A study in patients with extremity fractures. *J Orthop Trauma* 29:e198–e202.
52. Kimerling R, Clum GA, Wolfe J (2000) Relationships among trauma exposure, chronic posttraumatic stress disorder symptoms, and self-reported health in women: Replication and extension. *J Trauma Stress* 13:115–128.
53. Libow JA (1995) Munchausen by proxy victims in adulthood: A first look. *Child Abuse Negl* 19:1131–1142.
54. Thayer MK, Vaidya R, Langfitt M, Carroll EA, Cannada LK (2015) Functional outcomes after both bone forearm fractures in adults. *J Surg Orthop Adv* 24:164–169.
55. Rontgen V, et al. (2010) Fracture healing in mice under controlled rigid and flexible conditions using an adjustable external fixator. *J Orthop Res* 28:1456–1462.
56. Langgartner D, Füchsl AM, Uschold-Schmidt N, Slattery DA, Reber SO (2015) Chronic subordinate colony housing paradigm: A mouse model to characterize the consequences of insufficient glucocorticoid signaling. *Front Psychiatry* 6:18.
57. Singewald GM, Nguyen NK, Neumann ID, Singewald N, Reber SO (2009) Effect of chronic psychosocial stress-induced by subordinate colony (CSC) housing on brain neuronal activity patterns in mice. *Stress* 12:58–69.
58. Veenema AH, Reber SO, Selch S, Obermeier F, Neumann ID (2008) Early life stress enhances the vulnerability to chronic psychosocial stress and experimental colitis in adult mice. *Endocrinology* 149:2727–2736.
59. Bouxsein ML, et al. (2010) Guidelines for assessment of bone microstructure in rodents using micro-computed tomography. *J Bone Miner Res* 25:1468–1486.
60. Haffner-Luntzer M, et al. (2014) Midkine-deficiency delays chondrogenesis during the early phase of fracture healing in mice. *PLoS One* 9:e116282.
61. Sonntag KC, Woo TW (2018) Laser microdissection and gene expression profiling in the human postmortem brain. *Handb Clin Neurol* 150:263–272.
62. Ramakers C, Ruijter JM, Deprez RH, Moorman AF (2003) Assumption-free analysis of quantitative real-time polymerase chain reaction (PCR) data. *Neurosci Lett* 339:62–66.